Optimisation of Multi-Energy System Operation with Convex Efficiency Representation at Partial Loading

Optimisation of Multi-Energy System Operation with Convex Efficiency Representation at Partial Loading

Cristian Piran, Alessio Barale, Andrea Mazza, *Senior Member*, *IEEE*, and Gianfranco Chicco, *Fellow, IEEE*

***Abstract*—The optimal operation of multi-energy systems (MES) that supply a demand formed by different energy vectors can be determined based on a given objective function with the relevant constraints. An efficient approach formulated in the literature defines an optimisation model with linear constraints considering constant efficiency or constant coefficient of performance (*COP*) of the individual equipment. This paper extends this optimisation model by considering non-linear convex expressions of the equipment efficiencies and *COP*s. The optimisation with linear constraints is solved in an iterative way, by updating the efficiencies and *COP*s at each iteration until the convergence criterion is satisfied. The results of this approach are shown for a MES that supplies electricity, heat and cooling demand in representative cases for winter and summer periods. The relevant aspects are the possibility of determining more realistic operation costs, higher than the operation costs found with constant efficiencies when the efficiency of the equipment varies in a monotonic way. Conversely, with non-monotonic variations (e.g., for the *COP*, when the MES serves a cooling demand), the operation costs do not increase in all cases. Finding more realistic operation costs becomes crucial in MES applications with increasing electricity and gas prices, with higher correlations occurring at high price levels. Finally, a novel graphical method is presented to indicate the MES contributions equipment in serving electricity, heat and cooling demand, also showing the upward and downward flexibility due to energy shifting in the MES.**

***Index Terms*—Multi-energy system, Operation, Optimisation, Efficiency, Energy hub, Electricity prices, Gas prices.**

I. Introduction

THE energy sector is undergoing a remarkable transformation, driven by the current trends towards decarbonisation and recent challenges imposed by the very large changes in energy prices experienced in many countries [1]. In the energy transition process in progress, the deployment of multi-energy systems (MES) [2] provides viable options for the integrated use of different energy vectors in various applications in the industry, the tertiary sector, energy districts, and the evolving energy communities [3].

The studies on MES operation can be structured by resorting to the framework introduced under the name energy hub [4]. This framework includes a matrix-based model structurally similar for each MES component and the overall MES. This matrix model is based on the input-output relations between the vector of inputs $\mathbf{v}_{\text{in}}$ and the vector of outputs $\mathbf{v}_{\text{out}}$, established through the coupling matrix $\mathbf{C}_{\text{out,in}}$:

$$\mathbf{v}_{\text{out}} = \mathbf{C}_{\text{out,in}}\, \mathbf{v}_{\text{in}} \qquad (1)$$

If the relation (1) is written for a single MES component, the coupling matrix contains information on the efficiencies (for components that produce electricity and/or heat) or Coefficient of Performance (*COP*) for cooling production components.

On the other hand, if the relation (1) is written for the overall MES, the coupling matrix contains information on both the efficiencies and *COP*s of the individual components, as well as the topology of the interconnections among the components. If the output from a MES component is directed to more than one destination through a bifurcation point, the share of the output that reaches each destination is represented by the dispatch factors, which sum up to unity at each bifurcation point.

In the presence of multiple equipment in the MES, there are many ways to serve the multi-energy demand staring from the same supply systems. Different multi-energy flows are possible, in a way consistent with the technical characteristics of the equipment and with the topology of the interconnections. The dispatch factors may be taken as degrees of freedom to be used as decision variables in an optimisation procedure referring to a given objective function.

A major benefit of the energy hub model is that the relation (1) can be written for the overall MES by determining the coupling matrix entries directly by visual inspection. An automatic procedure for the symbolic construction of the coupling matrix of the overall MES has been formulated in [5]. However, with the use of dispatch factors in the determination of the overall coupling matrix, the consequent optimisation problem becomes non-linear, as some entries of the overall coupling matrix contain products of dispatch factors. In this case, the solution of the optimisation problem depends on the initial point considered, and multiple local optima could appear for different initial operating points. On these bases, a different solution was proposed [6] by avoiding the use of the dispatch factors and expressing the constraints with a linear formulation, provided that the efficiencies and *COP*s of the equipment are constant (i.e., equal to their values in rated conditions at full loading). Likewise, the automatic method developed to construct the overall coupling matrix described in [7] avoids the use of the dispatch factors and considers constant efficiencies and *COP*s.

The developments indicated above have provided an efficient way to address energy hub modelling with constant efficiencies and *COP*s. However, the actual efficiencies and *COP*s are not constant with respect to the loading level of the equipment. Hence, successive studies have incorporated variable energy efficiencies in the modelling. The typical solution adopted is the transformation of non-linear characteristics or constraints into linear segments by applying piecewise linear approximations ([8],[9]). The piecewise linear approximation requires the identification of the segments by

The authors are with Politecnico di Torino, Dipartimento Energia "Galileo Ferraris", Corso Duca degli Abruzzi 24, 10129 Torino, Italy (email: andrea.mazza@polito.it, gianfranco.chicco@polito.it).

Color versions of one or more of the figures in this article are available online at http://ieeexplore.ieee.org.

using a set of secondary variables, together with binary values introduced to represent the continuity of the segments. The number of segments can be chosen by considering the type of non-linearity of the curve to be linearised. The error shown in [9] depends on the number of segments used in the piecewise linearisation (requiring about 50 segments to substantially reduce the error) and the computation time increases more than linearly when the number of segments increases.

The piecewise linear approximation can provide an approximate representation of the non-linear efficiency and *COP* characteristics, at the expense of increasing the number of variables of the model. However, for the MES equipment the individual non-linear efficiency and *COP* curves drawn in function of the loading level are mostly smooth and convex.

On these bases, in [10] the MES representation used in the energy hub model has been formulated by keeping the efficiency and *COP* curves in their non-linear convex form and constructing an iterative procedure to solve the MES optimisation. This procedure iterates the solution of the optimisation model with linear constraints formulated in [6] by changing at each iteration the numerical values of efficiencies and *COP*s. This novel formulation is conceptually more accurate than assuming constant parameters or variable parameters based on piecewise linear approximations.

Executing the MES optimisation to find how the MES components operate at partial loading is also essential to determine an (optimal) baseline to be used for different purposes. One of the key aspects is to determine how the operating conditions could change depending on the characteristics of the equipment used. There are two main concepts to consider:

1. *Feasibility*: it is represented by the *feasibility region*, composed of all the operating points that can be reached through different combinations of equipment connected in the MES system. Feasibility is a *global* (i.e., referring to the whole region) and is generally considered a *static* (i.e., not depending on time) property in the multi-energy domain, even though time-dependent regions can be defined by taking into account the ramp-rate limits on the relevant quantities.
2. *Flexibility*: starting from a given operating point (baseline), the operational flexibility is assessed considering the *variations* that can be obtained in the MES until specific limit conditions are reached. The limit conditions must be addressed by considering the timing at which the variations can be applied, as different equipment has dedicated limitations to perform rapid changes, generally represented as ramp-rate constraints. Flexibility is a *local* (i.e., depending on the initial point) and *dynamic* (i.e., time-dependent) property in the multi-energy domain. For a variation of a single energy vector, flexibility is further divided into *upward* (with reduction of the input energy vector, i.e., with local generation increase) and *downward* (with increase of the input energy vector, i.e., with local generation reduction) [11].

The baseline is also used for determining the possible exploitation of the MES to provide *demand response* services [12] through internal energy shifting based on suitable incentives [13]. Profitable solutions can be found depending on the level of incentives and the costs to modify the baseline solution within the MES for changing the electricity input from (or output to) the electricity distribution system. The arbitrage opportunities that emerge in the MES are assessed by calculating the maximum profit that can be obtained from the application of energy-shifting actions in the MES and the corresponding Maximum Profit Electricity Reduction in case of reducing the electricity input [14].

The studies on the MES profitability are becoming increasingly important in a historical period in which the fluctuations of the energy prices are high, depending on many external conditions. In particular, since the year 2021 the prices of electricity and fuel (gas and others) are experiencing an unprecedented remarkable increase, with significant consequences on the entire energy sector. In such a situation, availability of a computational tool that provides meaningful results by representing the efficiency and *COP* variations of the MES components at partial loading is a valuable asset. The outcomes of the computational tool that provides the optimal solution for a given operating point can be then integrated into a time-domain analysis framework for a specified period of time with time steps with for the related demand variations. This framework includes the study concerning the role of MES flexibility and profitability under very high energy prices, in which using more accurate representations of the partial-loading efficiencies and *COP*s of the equipment by using the proposed optimisation is a considerable benefit.

This paper is the extended version of [10], with the following additional contributions:

- More details are shown on the solution process of the proposed MES optimisation in specific cases.
- Some notes on the convergence of the proposed overall optimisation process are added.
- More contents are included to show the correlation changes between electricity and gas prices for different levels of prices, with reference to real cases occurred in recent years.
- A novel graphical method is presented to identify the contributions of the MES components to serve electricity, heat and cooling load, extending the graphical method applied to electricity and heat load introduced in [11].

The next sections of this paper are organised as follows. Section II recalls the main aspects of MES modelling in the energy hub framework and the formulation of the MES optimisation with linear constraints for constant efficiencies and *COP*s, by identifying the types of variables used and the corresponding matrix formulation. Section III describes the extension of the optimisation model to the case with non-constant and convex representations of efficiencies and *COP*s of the MES components. Section IV illustrates the application of the proposed optimisation procedure to a MES in which the user multi-energy demand is defined in a given time period partitioned into successive time steps. Section V shows results referring to cases with different energy prices, including large variations in the electricity and gas prices. Section VI shows the application of the proposed graphical representation to show the contributions of MES components to serve multi-energy demand. The last section contains the concluding remarks.

II. Matrix Modelling of Multi-Energy Systems

A. MES Structure and Components

Without loss of generality, the concepts proposed in this paper are directly applied to the MES structure shown in Fig. 1, in which the MES serves the multi-energy demand (denoted as W_0 for electricity, Q_0 for heat, and R_0 for cooling) starting from

the inputs provided by the Electricity Distribution System (EDS) and the Fuel Distribution System (FDS). The MES demand is represented by given demand patterns referring to each time step considered inside the period of analysis. The demand can be represented in form of average power values or energy values at each time step (with an hourly time step, the numerical values coincide).

The MES contains the following equipment:

- The combined heat and power (CHP) unit, with fuel input F_{CHP} and simultaneous output of electricity W_{CHP} and heat Q_{CHP}. The rated values for the CHP are $W_{\mathrm{CHP}}^{(\mathrm{r})}$ for electricity and $Q_{\mathrm{CHP}}^{(\mathrm{r})}$ for heat, respectively. In the energy hub model, the CHP is characterised by electrical efficiency $\eta_{W,\mathrm{CHP}} = W_{\mathrm{CHP}}/F_{\mathrm{CHP}}$ and thermal efficiency $\eta_{Q,\mathrm{CHP}} = Q_{\mathrm{CHP}}/F_{\mathrm{CHP}}$.
- The auxiliary boiler AB, which serves as heat backup if the CHP is switched off or the heat demand at the thermal side of the CHP exceeds the thermal rating $Q_{\mathrm{CHP}}^{(\mathrm{r})}$.
- The electric heat pump EHP, which can supply either the heat or the cooling output (in different operating modes), with $COP_{Q,\mathrm{EHP}} = Q_{\mathrm{EHP}}/W_{\mathrm{EHP}}$ in heating mode and $COP_{R,\mathrm{EHP}} = R_{\mathrm{EHP}}/W_{\mathrm{EHP}}$ in cooling mode.
- The water absorption refrigerator group (WARG), which converts heat into cooling, with coefficient of performance $COP_{\mathrm{WARG}} = R_{\mathrm{WARG}}/Q_{\mathrm{WARG}}$.

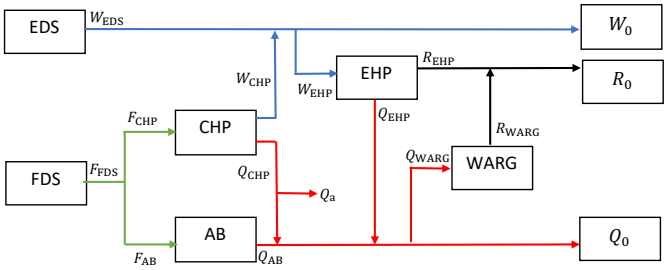

Fig. 1. MES equipment and interconnections.

B. Definition of the Variables of the Linearised Model

The variables included in the MES model are partitioned into the following vectors:

a) *Output* variables:

$$\mathbf{v}_{\mathrm{out}} = [W_0, \quad Q_0, \quad R_0]^{\mathrm{T}} \tag{2}$$

b) *Input* variables:

$$\mathbf{v}_{\mathrm{in}} = \left[F_{\mathrm{FDS}}, \quad W_{\mathrm{EDS}}^{(+)}, \quad W_{\mathrm{EDS}}^{(-)}\right]^{\mathrm{T}} \tag{3}$$

where F_{FDS} is the fuel supplied by the fuel distribution system, $W_{\mathrm{EDS}}^{(+)}$ is the electricity bought from the EDS, and $W_{\mathrm{EDS}}^{(-)}$ is the electricity sold to the EDS.

c) *Intermediate* variables, which include the outputs from every equipment (for the EHP, the variables Q_{EHP} or R_{EHP} could be used in alternative, when the EHP operates in heating mode or cooling mode, respectively):

$$\mathbf{v}_{\mathrm{imd}} = [W_{\mathrm{CHP}}, \quad Q_{\mathrm{CHP}}, \quad Q_{\mathrm{AB}}, \quad R_{\mathrm{EHP}}, \quad Q_{\mathrm{EHP}}, \quad R_{\mathrm{WARG}}]^{\mathrm{T}} \tag{4}$$

d) *Augmented* variables, introduced in each bifurcation with n branches to represent (n-1) degrees of freedom. A bifurcation occurs when the energy output from an equipment goes to two or more paths. Considering Fig. 1, the bifurcations occur for the fuel (the total fuel F_{FDS} bifurcates into F_{CHP} and F_{AB}), electricity (with the bifurcation into W_{EHP} and W_0), and heat (in the bifurcation into Q_{WARG} and Q_0, as well as in the bifurcation at the CHP output in which the part Q_{a} of the heat can be wasted to the ambient and the remaining heat goes forward):

$$\mathbf{v}_{\mathrm{aug}} = [F_{\mathrm{CHP}}, \quad W_{\mathrm{EHP}}, \quad Q_{\mathrm{WARG}}, \quad Q_{\mathrm{a}}]^{\mathrm{T}} \tag{5}$$

The contents of the vector $\mathbf{x} = \left[\mathbf{v}_{\mathrm{in}}^{\mathrm{T}}, \mathbf{v}_{\mathrm{aug}}^{\mathrm{T}}\right]^{\mathrm{T}}$ are unknown and are the decision variables of the problem. Conversely, in the hypothesis that there is no curtailment to the various types of energy supplied to the users, the contents of the output vector $\mathbf{v}_{\mathrm{out}}$ are known and do not depend on the multi-energy variables or parameters. Hence, these components remain constant, in such a way that the MES operation can be optimised without changing the user's multi-energy demand, i.e., without sacrificing the user's lifestyle and comfort.

The contents of the intermediate vector $\mathbf{v}_{\mathrm{imd}}$ are unknown; however, these contents represent output values that are bounded by the rated values of the equipment, that is:

$$\mathbf{v}_{\mathrm{imd}}^{(\mathrm{r})} = \left[W_{\mathrm{CHP}}^{(\mathrm{r})}, Q_{\mathrm{CHP}}^{(\mathrm{r})}, Q_{\mathrm{AB}}^{(\mathrm{r})}, R_{\mathrm{EHP}}^{(\mathrm{r})}, Q_{\mathrm{EHP}}^{(\mathrm{r})}, R_{\mathrm{WARG}}^{(\mathrm{r})}\right]^{\mathrm{T}} \tag{6}$$

C. Coupling Matrix and Related Partitions

The energy balances of the three energy vectors are written by visual inspection of the scheme represented in Fig. 1:

a) For electricity:

$$W_{\mathrm{EDS}} + \eta_{W,\mathrm{CHP}} \cdot F_{\mathrm{CHP}} - W_{\mathrm{EHP}} - W_0 = 0 \tag{7}$$

b) For heat:

$$\eta_{W,CHP} \cdot F_{CHP} - Q_a + \eta_{AB} \cdot (F_{FDS} - F_{CHP}) + \\ + COP_{Q,\mathrm{EHP}} \cdot W_{\mathrm{EHP}} - Q_{\mathrm{WARG}} - Q_0 = 0 \tag{8}$$

c) For cooling:

$$COP_{R,\mathrm{EHP}} \cdot W_{\mathrm{EHP}} + COP_{\mathrm{WARG}} \cdot Q_{\mathrm{WARG}} - R_0 = 0 \tag{9}$$

The matrix equation of the system is written in a compact form as in [6]:

$$\begin{vmatrix}\mathbf{v}_{\mathrm{out}} \\ \mathbf{v}_{\mathrm{imd}}\end{vmatrix} = \begin{vmatrix}\mathbf{C}_{\mathrm{out,in}} & \mathbf{C}_{\mathrm{out,aug}} \\ \mathbf{C}_{\mathrm{imd,in}} & \mathbf{C}_{\mathrm{imd,aug}}\end{vmatrix} \begin{vmatrix}\mathbf{v}_{\mathrm{in}} \\ \mathbf{v}_{\mathrm{aug}}\end{vmatrix} = \mathbf{C} \begin{vmatrix}\mathbf{v}_{\mathrm{in}} \\ \mathbf{v}_{\mathrm{aug}}\end{vmatrix} \tag{10}$$

where $\mathbf{C}_{\mathrm{out,in}}$ is the classical coupling matrix used in the energy hub model [4], and $\mathbf{C}$ is the augmented coupling matrix, which contains the augmented coupling submatrices $\mathbf{C}_{\mathrm{out,aug}}$ and $\mathbf{C}_{\mathrm{imd,aug}}$, as well as the submatrix $\mathbf{C}_{\mathrm{imd,in}}$ [6]. The entries of these matrices combine information on the efficiency and *COP* of the equipment with the topology of the interconnections inside the system.

For the MES equipment in Fig. 1, the augmented coupling matrix is written as follows:

$$\mathbf{C} = \begin{bmatrix} 0 & 1 & -1 & \eta_{W,\mathrm{CHP}} & -1 & 0 & 0 \\ \eta_{\mathrm{AB}} & 0 & 0 & \eta_{Q,\mathrm{CHP}} - \eta_{\mathrm{AB}} & COP_{Q,\mathrm{EHP}} & -1 & -1 \\ 0 & 0 & 0 & 0 & COP_{R,\mathrm{EHP}} & COP_{\mathrm{WARG}} & 0 \\ 0 & 0 & 0 & \eta_{W,\mathrm{CHP}} & 0 & 0 & 0 \\ 0 & 0 & 0 & \eta_{Q,\mathrm{CHP}} & 0 & 0 & 0 \\ \eta_{\mathrm{AB}} & 0 & 0 & -\eta_{\mathrm{AB}} & 0 & 0 & 0 \\ 0 & 0 & 0 & 0 & COP_{R,\mathrm{EHP}} & 0 & 0 \\ 0 & 0 & 0 & 0 & COP_{Q,\mathrm{EHP}} & 0 & 0 \\ 0 & 0 & 0 & 0 & 0 & COP_{\mathrm{WARG}} & 0 \end{bmatrix} \tag{11}$$

The first three rows of the matrix $\mathbf{C}$ contain the coefficients of the energy balances (7)–(9). The other rows contain the coefficients of the output-to-input relations for the individual equipment. The first three rows and the first three columns correspond to the entries of the submatrix $\mathbf{C}_{\mathrm{out,in}} \in \Re^{3,3}$. The

other submatrices have dimensions $\mathbf{C}_{\text{out,aug}} \in \Re^{3,4}$, $\mathbf{C}_{\text{imd,in}} \in \Re^{6,3}$, and $\mathbf{C}_{\text{imd,aug}} \in \Re^{6,4}$.

D. Optimisation Model with Linear Constraints

If all efficiencies and *COP*s are constant, considering an objective function $f(\mathbf{x})$, e.g., to minimise, it is possible to construct an optimisation model with linear constraints, which uses the sub-matrices of the matrix $\mathbf{C}$ as coefficients, as follows:

$$\min_{\mathbf{x}}\{f(\mathbf{x})\} \tag{12}$$
$$\text{s.t.} \quad \mathbf{v}_{\text{out}} - |\mathbf{C}_{\text{out,in}} \ \mathbf{C}_{\text{out,aug}}|\,\mathbf{x} = \mathbf{0}$$
$$\mathbf{v}_{\text{imd}}^{(\text{r})} - |\mathbf{C}_{\text{imd,in}} \ \mathbf{C}_{\text{imd,aug}}|\,\mathbf{x} \geq \mathbf{0}$$

The objective function can be for example the minimum operation cost, formulated taking into account the fuel price ρ_F, the price $\rho_{W,\text{buy}}$ of the electricity bought from the EDS, and the price $\rho_{W,\text{sell}}$ of the electricity sold to the EDS. In this case, the objective function can be expressed as:

$$f(\mathbf{x}) = \rho_F\, F_{\text{FDS}} + \rho_{W,\text{buy}}\, W_{\text{EDS}}^{(+)} + \rho_{W,\text{sell}}\, W_{\text{EDS}}^{(-)} \tag{13}$$

and is implemented with the additional constraints that return the unbounded electricity W_{EDS} and the constraints on its components:

$$W_{\text{EDS}} = W_{\text{EDS}}^{(+)} + W_{\text{EDS}}^{(-)} \tag{14}$$
$$W_{\text{EDS}}^{(+)} \geq 0 \tag{15}$$
$$-W_{\text{EDS}}^{(-)} \geq 0 \tag{16}$$

The objective function can be expressed in a linear form, by including the optimisation variables coefficients in the vector $\boldsymbol{\zeta} = \left[\rho_F,\ \rho_{W,\text{buy}},\ \rho_{W,\text{sell}}, 0,\ 0,\ 0,\ 0\right]^{\text{T}}$:

$$f(\mathbf{x}) = \boldsymbol{\zeta}^{\text{T}}\,\mathbf{x} \tag{17}$$

The presence of the minimum technical limits of the CHP (denoted as $W_{\text{CHP}}^{(\text{min})}$ on the electrical side and $Q_{\text{CHP}}^{(\text{min})}$ on the thermal side) requires the introduction of further constraints. Below the minimum technical limits of the CHP, the only feasible operating point if the switch-off condition. Therefore, the operating points of the CHP belong to two disconnected regions. This type of discontinuity is considered by introducing a binary variable u (equal to unity when the CHP is on and to zero when the CHP is off) [15]. The related inequalities are:

$$W_{\text{CHP}} \geq W_{\text{CHP}}^{(\text{min})} u \tag{18}$$
$$-W_{\text{CHP}} \geq -W_{\text{CHP}}^{(\text{r})} u \tag{19}$$
$$Q_{\text{CHP}} \geq Q_{\text{CHP}}^{(\text{min})} u \tag{20}$$
$$-Q_{\text{CHP}} \geq -Q_{\text{CHP}}^{(\text{r})} u \tag{21}$$

This optimisation problem is solved with any classical solver that handles linear objective functions and linear constraints, with upper and lower bounds on the variables.

III. Extension of the Optimisation Model to Consider Non-Constant Efficiencies and *COP*s

A. Non-Constant Efficiencies

When the efficiencies and *COP*s are constant, the optimisation model with linear constraints provides the optimal solution in a simple way. However, the actual efficiencies and *COP*s of the MES equipment are not constant. For a more realistic characterisation of the performance of the individual equipment, the hypothesis of constant efficiencies and *COP*s must be removed, especially when the output from the equipment is relatively low with respect to the rated output.

The typical efficiency curves of the equipment are drawn from experimental results available in the literature [16]-[19]. In particular:

a) For the AB, an expression that represents the AB efficiency η_{AB} in terms of the heat output Q_{AB}, the heat output level $q_{\text{AB}} = Q_{\text{AB}}/Q_{\text{AB}}^{(\text{r})}$, the AB losses $Q_{\text{AB}}^{(\text{losses})}$, and the relative AB losses $q_{\text{AB}}^{(\text{losses})} = Q_{\text{AB}}^{(\text{losses})}/Q_{\text{AB}}^{(r)}$ is [16][17]:

$$\eta_{\text{AB}} = \frac{q_{\text{AB}}}{q_{\text{AB}} + q_{\text{AB}}^{(\text{losses})}} \tag{22}$$

where the relative AB losses $Q_{\text{AB}}^{(\text{losses})}$ can be written in a polynomial form, considering the curve-fitting coefficients υ_0, υ_1 and υ_2:

$$q_{\text{AB}}^{(\text{losses})} = \upsilon_0 + \upsilon_1 \cdot q_{\text{AB}} + \upsilon_2 \cdot q_{\text{AB}}^2 \tag{23}$$

b) For the CHP, the partial-load electrical and thermal efficiencies ($\eta_{W,\text{CHP}}$ and $\eta_{Q,\text{CHP}}$, respectively) can be approximated in a linear way, or with a second-order model in the region of CHP operation [17][18]. The model is valid from the minimum technical limit to the rated conditions:

$$\eta_{W,\text{CHP}} = c_{W,0} + c_{W,1} \cdot W_{\text{CHP}} + c_{W,2} \cdot W_{\text{CHP}}^2 \tag{24}$$
$$\eta_{Q,\text{CHP}} = c_{Q,0} + c_{Q,1} \cdot Q_{\text{CHP}} + c_{Q,2} \cdot Q_{\text{CHP}}^2 \tag{25}$$

where the terms $c_{W,0}$, $c_{W,1}$, $c_{W,2}$, $c_{Q,0}$, $c_{Q,1}$, and $c_{Q,2}$ are curve-fitting coefficients. The minimum technical limit, for both electrical efficiency and thermal efficiency, is imposed in the optimisation procedure, so that there is no need to consider further values below the minimum technical limit.

B. Non-Constant *COP*

For the WARG, based on the typical partial-load performance, the *COP* variation with respect to the cooling output R_{WARG} and cooling output level $r_{\text{WARG}} = R_{\text{WARG}}/R_{\text{WARG}}^{(\text{r})}$ can be expressed as [17][19]:

$$COP_{\text{WARG}} = \frac{r_{\text{WARG}}}{r_{\text{WARG}} + \varsigma_0 + \varsigma_1 \cdot r_{\text{WARG}} + \varsigma_2 \cdot r_{\text{WARG}}^2} \tag{26}$$

where ς_0, ς_1 and ς_2 are curve-fitting coefficients. An interesting aspect for the WARG is that the maximum COP_{WARG} can be reached at a loading level lower than the rated output.

For the EHP, the main dependence of the *COP* is on temperature [18]. Therefore, at a given temperature level, for the application presented in this paper the *COP* is considered constant.

C. The Overall Optimisation Procedure

Considering the convex representations of the efficiencies and *COP*s at partial load, the linear optimisation procedure [6] is extended to the case with non-constant efficiencies and *COP*s. The overall optimisation procedure is formulated as an iterative process in which the optimisation (12) is solved, then the parameters are updated, and the process is repeated until the specific stop criterion is satisfied. The variables and parameters of the optimisation procedure are identified as follows:

$\mathbf{x} = [F_{\text{FDS}}, W_{\text{EDS}}, F_{\text{CHP}}, W_{\text{EHP}}, Q_{\text{WARG}}, Q_a]^{\text{T}}$, vector of the optimisation variables; and,

$\boldsymbol{\xi} = \left[\eta_{\text{AB}}, \eta_{e,\text{CHP}}, \eta_{\text{t,CHP}}, COP_{\text{WARG}}\right]^{\text{T}}$, vector of the variable parameters (efficiencies and *COP*). The EHP parameter is considered constant in this example.

Fig. 2 shows the conceptual scheme of the proposed approach. The main steps of the overall optimisation procedure are:

a) *Initial optimal solution*: the optimisation (12) of the multi-energy system operation is solved with constant efficiencies and *COP*s, equal to the rated values, to obtain the initial values of the optimisation variables.
b) *Efficiency and COP update*: calculation of the new efficiencies and *COP*s from the equations indicated in Section III.A and Section III.B, respectively.
c) *Iterative re-optimisation*: the optimisation (12) is executed again with the updated efficiencies and *COP*s; the steps b) and c) are repeated until the stop criterion is satisfied.
d) *Stop criterion*: the procedure stops when the maximum variation of the optimisation variables in two successive iterations is lower than the predefined tolerance ε.

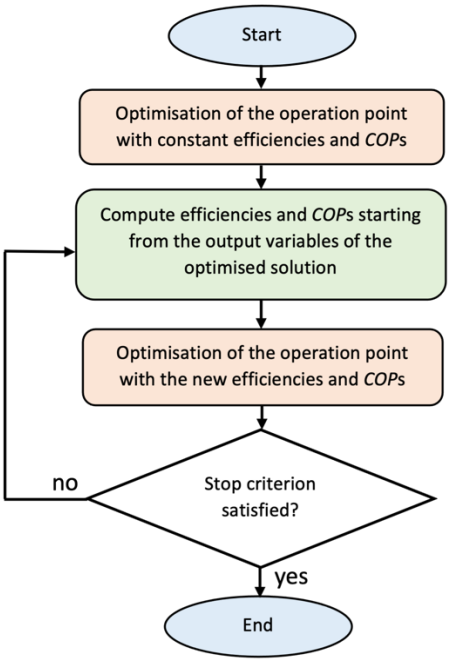

Fig. 2. Scheme of the procedure to execute the optimisation with non-constant efficiencies and *COP*s.

The optimisation problem considered has linear objective function, linear equality and inequality constraints, and upper and lower bounds on the problem variables. The optimisation problem has been solved by using the Matlab function linprog with the dual simplex algorithm [20].

D. Computational Burden

The computational burden of the iterative process executed at time step τ has been addressed by introducing the *average computation time per iteration* $\rho_{\mathrm{a}}^{(\tau)}$, considered in the cases with variable efficiency for the i = 1,…, $N_{\mathrm{v}}^{(\tau)}$ iterations with computation time $t_{\mathrm{v},i}^{(\tau)}$ at iteration i:

$$\rho_{\mathrm{a}}^{(\tau)} = \sum_{i=1}^{N_{\mathrm{v}}^{(\tau)}} t_{\mathrm{v},i}^{(\tau)} \qquad (27)$$

E. Convergence Properties

The overall optimisation procedure includes a first phase of assignment of the rated efficiencies and *COP*s, followed by the optimisation (12) that can be executed with any instance of the efficiencies and *COP*s, provided that no limit is introduced to the entries of the input variables. For electricity, the terms $W_{\mathrm{EDS}}^{(+)}$ and $W_{\mathrm{EDS}}^{(-)}$ have no upper bound, as it is expected from the correct design of the electricity supply network. Therefore, the electricity input from and output to the EDS are not bounded. Likewise, for fuel, the term F_{FDS} has no upper bound, meaning that the FDS has no limit to the fuel supply provision. To complete the view, the variable Q_a encompasses the case in which part of the CHP heat output is wasted off to the ambient.

On these bases, the overall optimisation procedure sketched in Fig. 2 is based on the augmented coupling matrix $\mathbf{C}(\boldsymbol{\xi})$, in which the entries of the vector $\boldsymbol{\xi}$ change in a convex way. The related linear optimisation problem has both equality and inequality constraints, with convex variation of the parameters in those constraints. To the authors' knowledge, there is no general formal proof of convergence for this class of problems. In [9] the non-linear efficiencies are handled through piecewise linear approximations, which can be used with any kind of functions, convex or not convex, and no convergence property has been discussed. However, with non-convex representations of the efficiencies or *COP*s there could be issues in the convergence of the solution process. The use of convex models for efficiencies and *COP*s proposed in this paper conceptually improves the convergence of the solution process. Furthermore, the comparison of the proposed approach with [9] is not an issue, as in general piecewise linear representations should be compared with the non-linear version to justify the reasonable choice of the number of piecewise segments, and not vice versa.

F. Graphical Procedure to Represent the Operating Conditions

When the operating conditions have been identified (for example, in an optimal way, or in other cases), a specific graphical procedure is presented to represent the contributions of the various components to serve the multi-energy demand. The concepts outlined in [11] for electricity and heat are extended for the first time to the overall representation of contributions referring to electricity, heat and cooling demand.

The graphical output is drawn in two dimensions, with electricity and heat on the horizontal and vertical axes, respectively. The steps of the procedure are:

1. Draw the feasibility region of the MES considering the technical limits of EDS, CHP and AB.
2. Introduce the point (W_0, Q_0) that indicates the electricity and heat demand of the user.
3. Add to the point (W_0, Q_0) the range of values that represent the electricity and heat needed to supply of the cooling demand from EHP and WARG, respectively. To guarantee feasibility, the resulting range of operating conditions must remain inside the feasibility region.
4. Draw the CHP contribution, which intersects the range of operating condition found in the previous step. The intersection between the CHP characteristic and the range of operating conditions defines the operating point. The CHP characteristic is introduced together with its horizontal and vertical axes; the location of the axes is used to specify the contributions of the supply systems to serve the multi-energy demand (next steps).

5. Identify the contributions of CHP and EDS to serve the electrical part of the multi-energy demand: the EDS contribution is found as the distance between the vertical axis of the overall figure and the vertical axis of the CHP contribution. The contribution of the CHP is identified on the horizontal axis of the CHP characteristic.
6. Identify the contributions of CHP and AB to serve the thermal part of the multi-energy demand: the AB contribution is found as the distance between the horizontal axis of the overall figure and the horizontal axis of the CHP contribution. The contribution of the CHP is identified on the vertical axis of the CHP characteristic.

Examples of application are shown in Section VI.

IV. Case Study Applications

A. MES Data

The MES system shown in Fig. 1 is considered, with the sizes and rated values of efficiencies and *COP*s reported in Table I. The convex representations of the efficiencies of the CHP and AB and of the *COP*s of the WARG presented in Section III.A are formulated with the curve-fitting coefficients indicated in Table II and depicted in Fig. 3.

For the CHP, the electrical and thermal efficiencies are defined only starting from the minimum technical limit, as below that limit the CHP is switched off by setting the binary variable u to zero in the equations (10) and (20). As such, the CHP efficiency characteristics are convex in the range of CHP operation.

TABLE I. Rated Values for the Equipment Considered

	***W*,CHP**	***Q*,CHP**	**AB**	**WARG**	***Q*,EHP**	***R*,EHP**
size [kW]	300	450	800	400	400	400
efficiency	0.3	0.45	0.85	-	-	-
COP	-	-	-	0.65	3	3

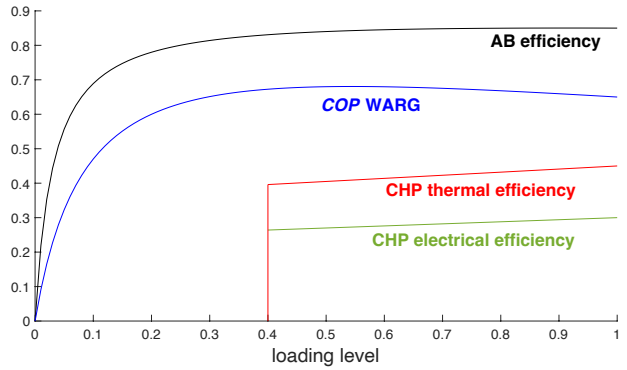

Fig. 3. Variable efficiencies and *COP* of the equipment.

TABLE II. Curve Fitting Coefficients

***W*,CHP**	***Q*,CHP**	**AB**	**WARG**
$c_{W,0} = 0.24$ $c_{W,1} = 0.06$ $c_{W,2} = 0$	$c_{Q,0} = 0.36$ $c_{Q,1} = 0.09$ $c_{Q,2} = 0$	$\upsilon_0 = 0.0347$ $\upsilon_1 = 0.1005$ $\upsilon_2 = 0.0413$	$\varsigma_0 = 0.0987$ $\varsigma_1 = 0.1067$ $\varsigma_2 = 0.3331$

The application is executed by considering two representative days belonging to different seasons, with the corresponding electrical, heating and cooling demand shown in Fig. 4, taken from realistic patterns of multi-energy loads in commercial sites.

The electricity and fuel prices reported in Fig. 5 are taken from real situations in two selected days:

- *winter day*, with prices on 13 January 2023;
- *summer day*, with prices on 24 August 2023.

In both cases, the price $\rho_{W,\text{sell}}$ of the electricity sold to the EDS is assumed to be one third of the price $\rho_{W,\text{buy}}$ of the electricity bought from the EDS. This assumption is used in Section IV.B for presenting the results and is then removed in the sensitivity analysis illustrated in Section IV.C, which is based on the ratio $\rho_{\text{EDS,ratio}}$ between the price of electricity sold and bought, defined as:

$$\rho_{\text{EDS,ratio}} = \frac{\rho_{W,\text{sell}}}{\rho_{W,\text{buy}}} \tag{28}$$

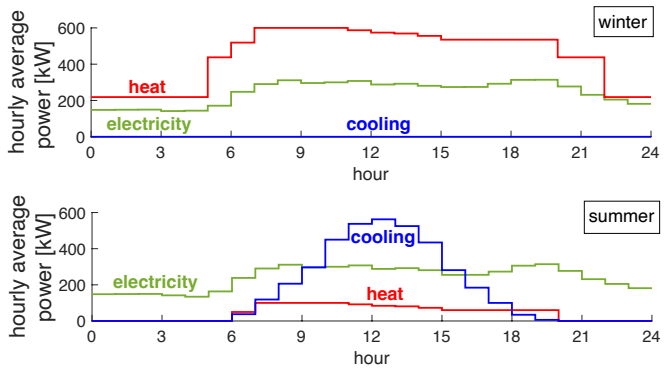

Fig. 4. Demand of electricity, heat and cooling in the winter and summer days.

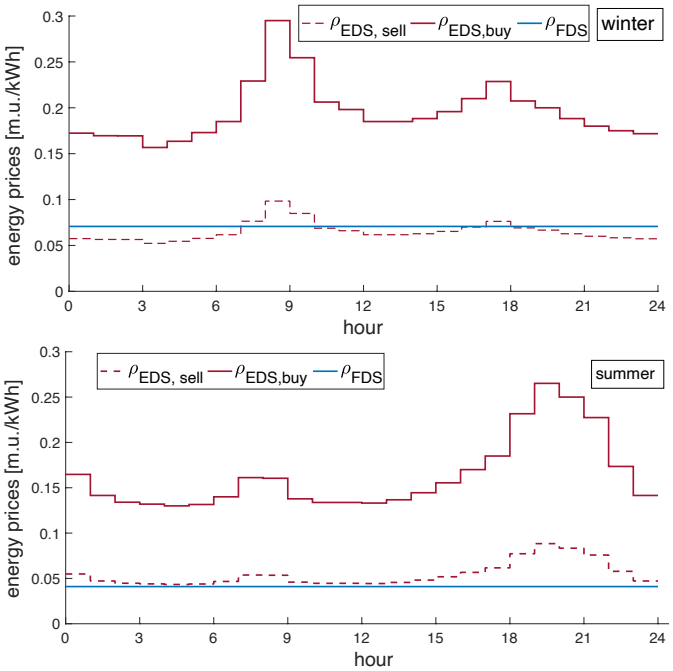

Fig. 5. Energy prices in the winter and summer days (m.u.: monetary units).

B. Optimisation Results in the Selected Days

The objective function (13) is minimised hour by hour by applying the constraints indicated in Section II.D. In all the optimisations, the efficiencies and *COP*s in the first iteration are initialised at rated values, while in the successive iterations the initial efficiencies and *COP*s are set to the values obtained at the previous iteration. The tolerance for the stop criterion is set to 10^{-5}. In addition to the number of iterations in the optimisation with variable efficiencies and *COP*, the average

computation time per iteration, defined in Section III.D, has been determined[1].

B.1. Results for the selected winter day

In the selected winter day, there is no cooling load and the only thermal equipment used are the CHP and the AB. The efficiencies of the CHP and AB are variable in a monotonic way, with the maximum value at rated conditions (i.e., at unity loading level). Then, with variable efficiencies at partial load, any operating point different from the rated conditions corresponds to lower efficiencies, leading to higher fuel consumption and related higher costs. The real cost is then always underestimated when using constant efficiencies.

From Fig. 6, the number of iterations varies from 2 to 3 and the average time per iteration has limited variations during the hours. From the hourly operation costs shown in Fig. 7, the daily costs calculated by considering variable efficiencies (1620.34 m.u.) are 3.9% higher than the corresponding daily costs determined with constant efficiencies (1556.65 m.u.). The maximum hourly cost difference (4.90 m.u.) appears at hour 6 am. In addition, the hourly cost difference is calculated by dividing the hourly cost difference by the hourly cost at variable efficiency, at each hour, and the maximum per cent hourly cost difference is 11% at hour 4 am.

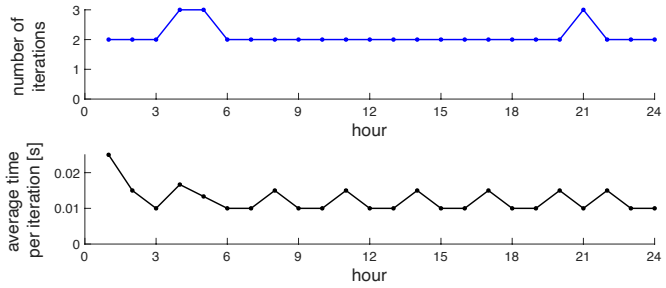

Fig. 6. Winter period: number of iterations and average time per iteration for the optimisation with variable efficiencies.

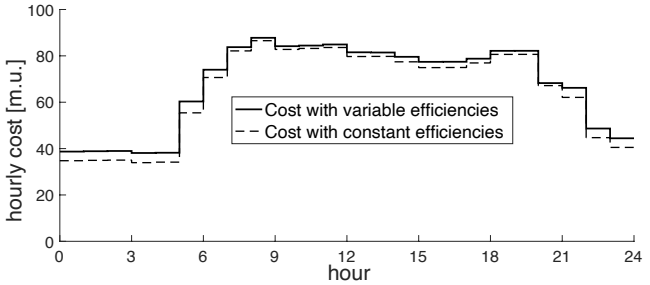

Fig. 7. Winter period: operation costs with constant and variable efficiencies.

B.2. Results for the selected summer day

During the summer, in some hours both the heat and cooling demands are null, as shown in Fig. 4. In these cases, the CHP could be switched off to serve the electrical demand from the EDS, with no need for executing the optimisation. However, since the gas price is relatively low, optimal solutions have been found at some hours in which the CHP is in operation to serve the electrical demand and even to sell the excess of electrical output to the EDS. In these hours, when the CHP operates at full loading, the same solution appears with constant or variable CHP efficiencies. Then, the results in Fig. 8 are reported for all the hours of the day.

In the central hours of the day, the number of iterations is higher than in the winter period, mainly because of the effect of serving the cooling load. In particular, the convex characteristic of the *COP* of the WARG is not monotonic and has a maximum at an intermediate loading level. In this case, there could be an increased number of iterations until stabilisation of the solution, in any case without large fluctuations in the results (specific details are shown in [10]). For example, at hour 11 am the *COP* of the WARG passes from the initial (rated) value 0.65 to 0.6692 at the second iteration and converges to the final value 0.6681 at the 6th iteration.

One of the effects of using a WARG with *COP* at partial loading higher than at rated conditions is the occurrence of a few cases in which the costs with variable efficiencies and *COP* are lower than the costs with constant efficiencies and *COP* in some central hours of the day (Fig. 9). In these cases, the WARG operates with higher *COP* with respect to the rated value and the use of non-constant *COP* allows highlighting the effectiveness of this solution.

Overall, the daily costs calculated by considering variable efficiencies and *COP* (843.14 m.u.) are still slightly higher than the corresponding daily costs determined with constant efficiencies and *COP* (831.14 m.u.), with a cost increase of 1.4%.

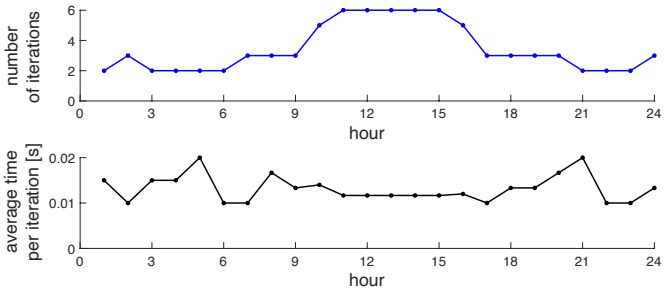

Fig. 8. Summer period: number of iterations and average time per iteration for the optimisation with variable efficiencies and *COP*.

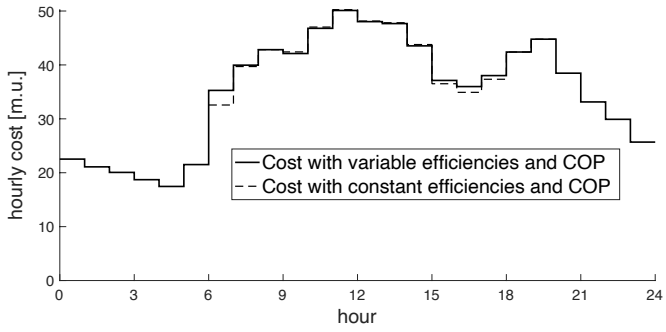

Fig. 9. Summer period: operation costs with constant and variable efficiencies and *COP*.

C. Sensitivity Analysis with Variable Gas Prices and Electricity Selling Price

The results shown above are based on the actual data of electricity and gas prices for the corresponding days, with the further hypothesis that the $\rho_{EDS,ratio}$ defined in (28) is equal to

[1] The simulations have been carried out on a MacBook Pro laptop with 2.3 GHz Intel Core i9 8 core processor and 16 GB RAM. If more executions are launched to find the same solution, the computation time is not always equal, and its variability is more evident being the computation times at the level of hundredths of seconds. As such, the average computation time per iteration has been shown to represent the indicative computational burden.

1/3. Moreover, in the cases analysed the gas prices, although taken from real cases, were relatively low. The whole calculations have been repeated for different values of the $\rho_{EDS,ratio}$ and with different gas prices, maintaining the same price for the electricity bought from the EDS. The per cent increase of the total daily cost in the solution with variable efficiencies and *COP* with respect to the solution with constant efficiencies and *COP* are reported in Fig. 10. The main remarks on the results shown are:

1. In the winter day, the per cent cost increase is mostly higher than in the summer day. This is due to the operation of CHP and AB at efficiencies not higher than the rated value, thus requiring more gas input at partial loading. In the summer day, the WARG could operate at *COP* higher than the rated value, with less heat input needed at the same loading. In this way, the savings on the WARG side mitigate the increased input for the operation of CHP and AB, resulting in a lower total cost increase with respect to the winter day.
2. When the gas price is very low and $\rho_{EDS,ratio} > 0$, the thermal side can be exploited more intensively. It could even happen that in the presence of electrical demand only (a condition that could require only the electricity input from the EDS, with the CHP switched off), the optimal solution for the hourly cost requires producing electricity with the CHP while wasting heat to the ambient[2].
3. When the gas price becomes relatively high, the electricity is bought from the EDS more intensively, and electricity is no longer sold to the EDS. As shown in Fig. 10, in the summer day, when the gas price is higher than about 0.07 m.u./kWh, the cost increase is the same for all cases of $\rho_{EDS,ratio}$. Also, in the winter day the solutions with relatively high gas price become independent of $\rho_{EDS,ratio}$.

The above considerations are valid in qualitative way, while they quantitatively depend on the specific day and data, including the fluctuations in time of the electricity price.

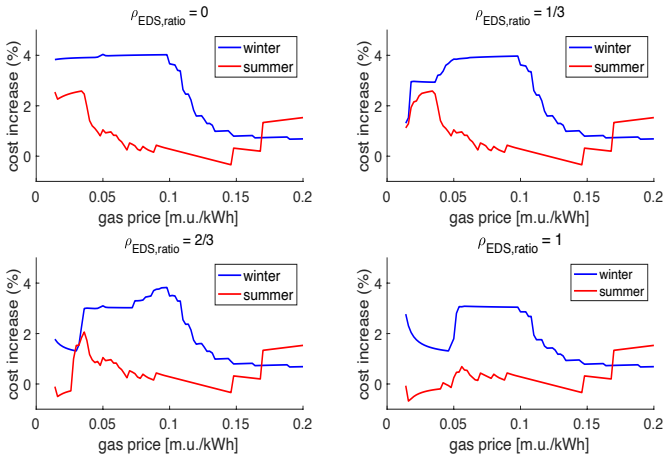

Fig. 10. Per cent total daily cost increase in the solutions with variable efficiencies and *COP* with respect to the solutions with constant efficiencies and *COP* by considering changes in the gas prices and different values of $\rho_{EDS,ratio}$.

V. Energy Price Variations and Impacts on the Operational Costs

A. Evolution of the Electricity and Gas Prices

Large variations in the energy prices have been experienced in the last years and are still continuing. Fig. 11 shows the fluctuations of the gas price in Italy in the years from 2019 to 2022 on a daily basis. To establish the price for each day, the mean value of all the negotiations closed over the Day-Ahead Market and the Intra-day Market have been considered. It can be noticed the remarkable rise of the price during 2021, with a series of peaks reached during 2022.

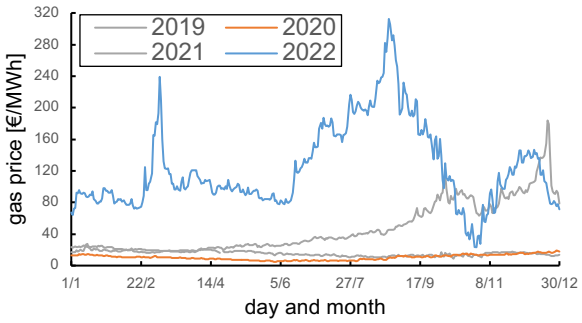

Fig. 11. Daily evolution of the gas price in Italy from 2019 to 2022.

Fig. 12 displays the evolution of the hourly price of electricity denoted as *SNP* ("Single National Price", from the Italian acronym *PUN* - Prezzo Unico Nazionale) during the same period of Fig. 11. The electricity price follows the gas price trend, with additional the fluctuations on an hourly basis.

To further understand the meaning of the increase of the prices, the gas and electricity prices are analysed through linear regression. The outcomes are shown in Fig. 13. The results are displayed separately for each year, keeping the same scales in each graph to have a clearer visual impact.

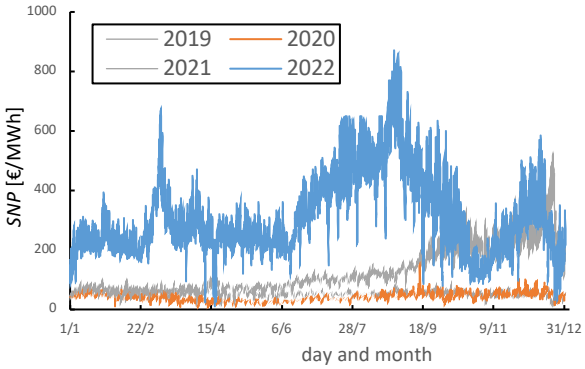

Fig. 12. Evolution of the hourly *SNP* in Italy from 2019 to 2022.

For the *SNP*, the daily value has been used, obtained by computing for each day the mean of the hourly prices reported in Fig. 12. The blue points display values of the two variables for every day considered. The red line shows the straight line corresponding to the best linear regression, indicating the corresponding R^2 value. The years 2021 and 2022 turn out as the most significant years, showing how for high price changes the two prices tend to be strongly correlated (high R^2 values),

[2] The solution with heat wasted to the ambient can become optimal when the objective function is the operation cost and there is no penalty for the energy wasted off, while would not be optimal with an objective function based on energy saving.

while in the years 2019 and 2020, with relatively low variations, the correlation is significantly weaker (low R^2 values).

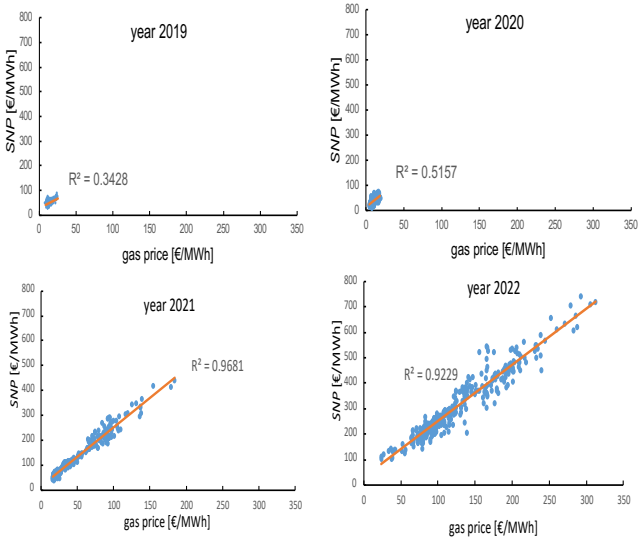

Fig. 13. Correlations between electricity and gas prices over the years 2019-2022.

B. *Example for a Selected Day*

To assess the MES operation in a case with significant electricity price variations, the day 7th February 2021 (Sunday) is the day with the highest relative change in electricity prices during the two years 2021 and 2022 (excluding the Christmas and Easter periods in Italy). The electricity and gas prices in this day are shown in Fig. 14. The selected day has an important decrease in electricity price early in the morning, followed by a steep rise during the morning, a second decrease during the afternoon and a second increase in the evening, reaching the peak at hour 20:00. The gas price (indicated as fuel price in the figure) is fixed. These variations cause a big change in the ratio between gas and electricity prices.

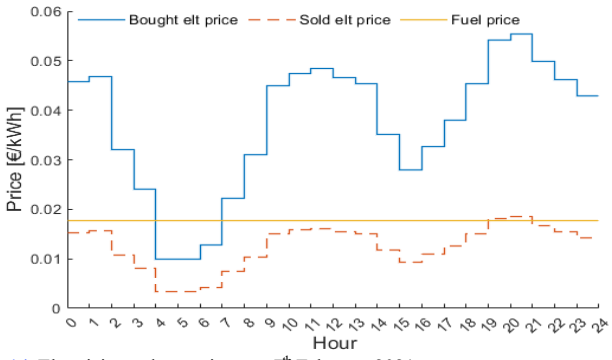

Fig. 14. Electricity and gas prices on 7th February 2021.

Fig. 15 shows the evolution of the energy demand during the considered day, taking into account the occurrence of a winter weather. Electricity and heat feature a base load during the night, while the cooling load is other than zero only during the central hours. The heat demand reaches the peak during the morning, whereas the electrical demand reaches the peak during the evening.

Fig. 16 shows, hour by hour, the results of the optimisation process in the selected MES. The energy values for the two grids, EDS and FDS, are displayed on the left vertical axis. It can be noticed that it is better to absorb a high quantity of gas, maintaining limited the electricity input. The only exception is on the early morning hours, in which the low electricity price makes it particularly convenient to buy electricity. The total cost of the energy bought on an hourly basis is displayed on the right vertical axis. During the drop of the electricity price the total cost declines, while during the central hours, with the increase of the demands, the total cost rises quickly and remains almost constant.

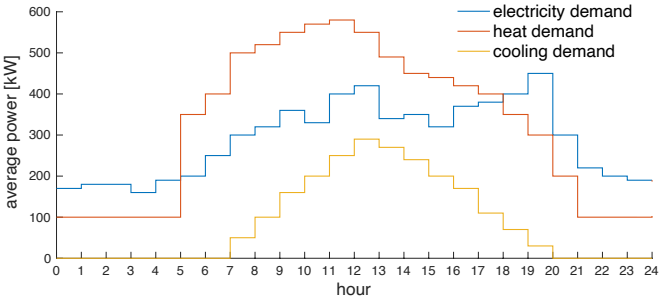

Fig. 15. Evolution of the demand during the selected day.

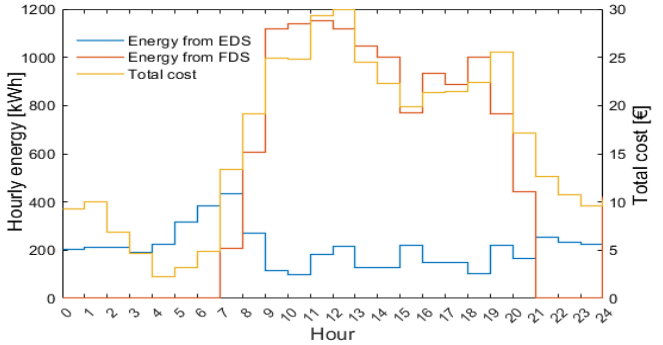

Fig. 16. Optimal cost and related electricity and fuel absorbed during the day.

VI. Graphical Representations of MES Feasibility Regions and Flexibility

A. *Feasibility Regions*

Let us consider the operational characteristics of the MES components (EDS, CHP and AB) shown in Fig. 17 on the left, from the data reported in Table I. The feasibility region for the system under analysis (Fig. 17 on the right) is determined through the application of Minkowski sum concepts [11]. The feasibility region represents all the operational points that can be reached from the outputs of CHP and AB, and from the electrical output from or input to the EDS. Serving the cooling demand through the EHP is seen as part of the electrical output of EDS and CHP. Likewise, serving the cooling demand through the WARG is seen as part of the heat output from the AB and the CHP. The filled area corresponds to the operational points that can be reached only with the CHP not in operation.

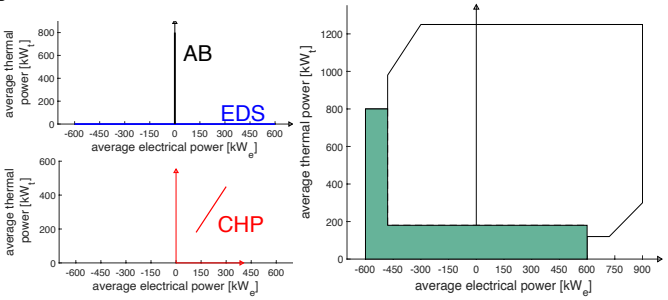

Fig. 17. Operational ranges of the EDS, AB and CHP and feasibility region for the average electrical and thermal powers.

A further specific characterisation of the electrical and thermal inputs needed to serve the cooling demand is represented in Fig. 18. For different values of the cooling demand $R_0 = R_{EHP} + R_{WARG}$, considering the *COP*s variable with the loading level of the EHP and WARG, respectively, the horizontal axis reports the electrical input to the EHP, $W_{EHP} = R_{EHP}/COP_{EHP}$, and the vertical axis reports the heat input to the WARG, $Q_{WARG} = R_{WARG}/COP_{WARG}$.When the cooling demand is 800 kW_c (i.e., the sum of the rated cooling outputs of EHP and WARG), there is a unique possibility to serve the cooling demand at full loading of EHP and WARG. When the cooling demand is lower than 800 kW_c, there are ranges of possible combinations to serve the demand through EHP and WARG, exemplified in the figure for certain values of R_0.

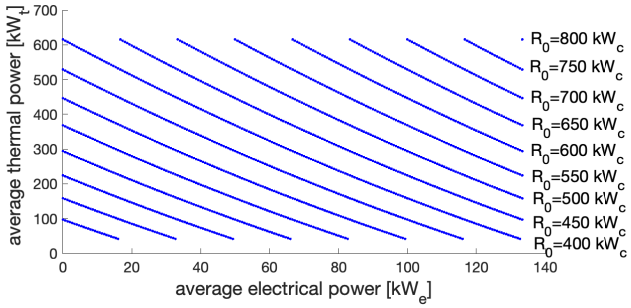

Fig. 18. Electrical input from the EHP and thermal input from the WARG to supply the cooling demand.

B. *Graphical Representation of the Operating Point*

The results of the graphical procedure described in Section III.F are presented in Fig. 19, considering the values at hour 10 am from Fig. 4. The corresponding graphical representation is shown in Fig. 20, highlighting the contributions of CHP and EDS.

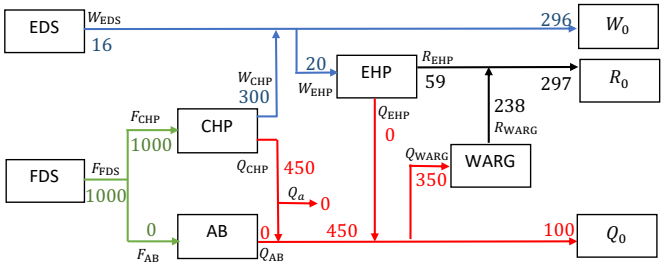

Fig. 19. Solution of the optimisation with variable efficiencies at hour 10 am.

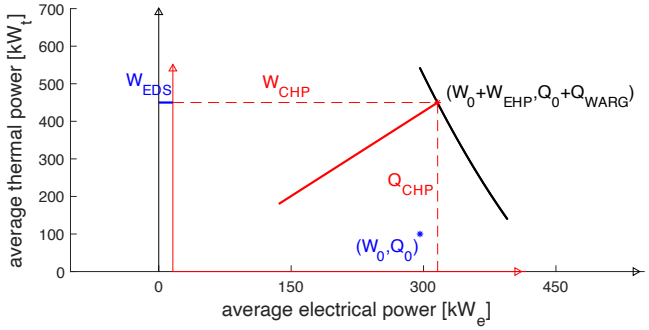

Fig. 20. Graphical representation of the MES operating point and of the contributions from the EDS, AB and CHP components at hour 10 am.

C. *Operational Flexibility*

Within the framework shown in the previous sections, it is possible to identify the upward and downward flexibility that can be provided by the MES in different cases, with regards to:

a) The *CHP operation*, considering the CHP in operation between its technical limits, or including the case in which the CHP can be switched off.

b) The *MES demand*, considering that the demand remains unchanged (so that the user is not affected by the internal redistribution of the energy flows), or including the case in which the demand can be curtailed.

To represent the maximum upward and downward flexibility conditions on the electrical side, two examples are shown below, starting from the operation point (baseline) at hour 10 am. The first example (Fig. 21) shows the conditions of maximum upward flexibility due to the maximum reduction of the electricity supply from the EDS. The electrical input to the EHP is reduced to zero, and the AB supplies the extra heat needed to serve the cooling demand R_0. The CHP remains at its full output (300 kW_e) to serve the electrical demand (296 kW_e) and send the excess of electricity production (4 kW_e) back to the EDS. The upward flexibility is then 16-(-4)=20 kW_e.

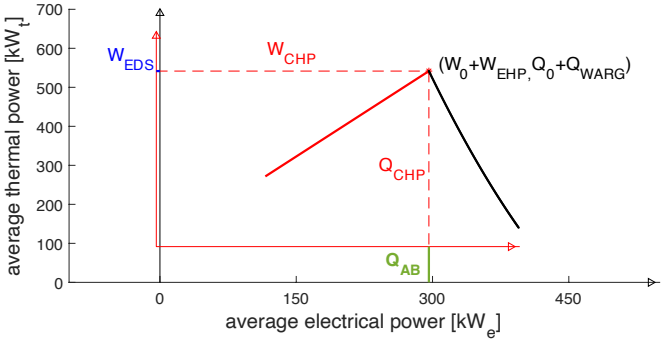

Fig. 21. Graphical representation of the maximum upward flexibility condition on the electrical side at hour 10 am.

The second example (Fig. 22) shows the condition of maximum downward flexibility with CHP in operation. This case corresponds to the maximum distance between the vertical axis of the CHP and the vertical axis of the system. The CHP minimum technical limit (120 kW_e) is located onto the black curve that corresponds to supplying the cooling demand. Since the thermal CHP output cannot be negative, the horizontal axis of the CHP is limited to the horizontal axis of the system and the operating point cannot reach the lower point of the black curve. Thereby, the maximum electrical input from the EDS is 263.5 kW_e, and the downward flexibility (expressed in absolute value) is |16-263.5| = 247.5 kW_e. If the CHP is switched off, the EDS can supply the total electrical demand (including the HEP input), reaching the lower point of the black curve, with $W_{EDS} = W_0 + R_0/COP_{EHP} =$ 395 kW_e. The corresponding maximum downward flexibility is |16-395| = 379 kW_e.

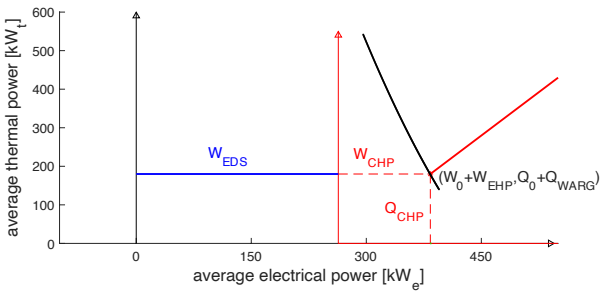

Fig. 22. Graphical representation of the maximum downward flexibility condition on the electrical side at hour 10 am.

VII. Conclusions

In MES optimisation, the representation of constant efficiencies and *COP*s of the equipment is a limiting aspect, even though an efficient procedure can be set up to solve the linearised energy hub model when constant efficiencies and *COP*s are assumed. In this paper, the optimisation model with linear constraints has been extended to consider non-constant efficiencies and *COP*s, represented through convex expressions at partial loading in the feasible region of operation. These convex expressions are continuous and do not require approximate piecewise linear representations. The optimisation problem is solved in an iterative way, by updating the efficiencies and *COP*s after each solution of the linear optimisation problem, until reaching the final convergence. The proposed procedure converges in a relatively low number of iterations also when the stop criterion has a small tolerance.

The sensitivity analyses highlighted that, generally, the MES configuration considered presents higher costs when the variable efficiencies and *COP* are included in the model than considering constant efficiencies and *COP*. In particular, the MES configuration presents higher cost increase at variable efficiencies and *COP* in winter than in summer, because of the typical monotonically decreasing nature of the efficiencies at partial loading of AB and CHP (requiring more input fuel). During the summer, the cost increase is less evident thanks to the operation of the WARG with higher *COP*, which partially balances the increase of input fuel of CHP and AB. Regarding the cost of gas and electricity prices, on the one hand, the presence of very low gas prices in some cases results in the convenience of using the CHP also when little or no heating load exists, due of the absence of any economic penalisation applied to the wasted heat. On the other hand, when the gas price is very high, it could become more convenient to use more electricity from the EDS.

Availability of more accurate data on the equipment efficiency and *COP* in the proposed optimisation approach is a valuable asset to reach more realistic results, especially in the recent context of unprecedented high and highly correlated electricity and gas prices.

The proposed procedure has been applied to the optimisation of the MES operation in different time steps, with electricity, heat and cooling patterns, and different energy prices. For easier visualisation of the results, a novel graphical procedure has been introduced to show the contributions of the MES components in serving the multi-energy demand. Finally, starting from a baseline formed in the optimal MES operating conditions, it has been shown how to identify the upward and downward flexibility that can be obtained in the MES through energy shifting applied to change the electricity input from or output to the EDS.

In the work in progress, the proposed optimisation procedure is being applied to the study of MES operation within emergent energy frameworks, such as local energy markets and multi-carrier energy communities.

References

[1] N. Fabra, “Reforming European electricity markets: Lessons from the energy crisis,” *Energy Economics*, vol. 126, ref. 106963, 2023.
[2] P. Mancarella, “MES (multi-energy systems): an overview of concepts and evaluation models,” *Energy*, vol. 65, pp. 1–17, 2014.
[3] E.A. Martinez Cesena, E. Loukarakis, N. Good and P Mancarella, “Integrated electricity-heat-gas systems: techno-economic modeling, optimization, and application to multienergy districts,” *Proceedings of the IEEE*, vol. 108 (9), pp. 1392–1410, 2020.
[4] M. Geidl, G. Koeppel, P. Favre-Perrod, B. Klockl, G. Andersson and K. Frohlich, “Energy hubs for the future,” *IEEE Power & Energy*, vol. 5 (1), pp. 24–30, 2007.
[5] G. Chicco and P. Mancarella, “Matrix modelling of small-scale trigeneration systems and application to operational optimization,” *Energy*, vol. 34 (3), pp. 261–273, 2009.
[6] Y. Wang, J. Cheng, N. Zhang and C. Kang, “Automatic and linearized modeling of energy hub and its flexibility analysis,” *Applied Energy*, vol. 211, pp. 705–714, 2018.
[7] Y. Wang, N. Zhang, C. Kang, D.S. Kirschen, J. Yang and Q. Xia, “Standardized matrix modeling of multiple energy systems,” *IEEE Trans. on Smart Grid*, vol. 10 (1), pp. 257–270, 2019.
[8] M.R. Almassalkhi and A. Towle, “Enabling city-scale multi-energy optimal dispatch with energy hubs,” *2016 Power Systems Computation Conference (PSCC)*, Genoa, Italy, 2016, pp. 1-7.
[9] W. Huang, N. Zhang, Y. Wang, T. Capuder, I. Kuzle and C. Kang, “Matrix modeling of energy hub with variable energy efficiencies,” *Electrical Power and Energy Systems*, vol. 119, art. 105876, 2020.
[10] C. Piran, A. Mazza and G. Chicco, “Operational Strategies for Serving the Multi-Energy Demand,” *Proc. International Conference on Smart Energy Systems and Technologies (SEST 2022)*, Eindhoven, The Netherlands, 5-7 September 2022.
[11] G. Chicco, S. Riaz, A. Mazza and P. Mancarella, “Flexibility from Distributed Multienergy Systems,” *Proceedings of the IEEE*, vol. 108 (9) pp. 1496-1517, 2020.
[12] Y. Zhao, C. Wang, Z. Zhang and H. Lv, "Flexibility Evaluation Method of Power System Considering the Impact of Multi-Energy Coupling," *IEEE Trans. on Industry Applications*, vol. 57, no. 6, pp. 5687-5697, 2021.
[13] P. Mancarella and G. Chicco, “Real-Time Demand Response from Energy Shifting in Distributed Multi-Generation”, *IEEE Trans. on Smart Grid*, vol. 4 (4), pp. 1928–1938, 2013.
[14] P. Mancarella, G. Chicco and T. Capuder, “Arbitrage opportunities for distributed multi-energy systems in providing power system ancillary services,” *Energy*, vol. 161, pp. 381-395, 2018.
[15] J. Hinker, H. Knappe and J.M.A. Myrzik, “Precise assessment of technically feasible power vector interactions for arbitrary controllable multi energy systems,” *IEEE Trans. on Smart Grid*, vol. 10 (1), pp. 1146-1155, 2019.
[16] A. Bejan, G. Tsatsaronis, and M. Moran, *Thermal design and optimization*, John Wiley and Sons, New York, 1996.
[17] P. Mancarella and G. Chicco, *Distributed multi-generation systems: energy models and analyses*, Nova Science Publishers, New York, 2009.
[18] J.F. Kreider (editor), *Handbook of Heating, Ventilation and Air Conditioning*, CRC Press, Boca Raton, FL, 2001.
[19] H. Li, R. Nalim, and P.A. Haldi, “Thermal-economic optimization of a distributed multi-generation energy system – A case study of Beijing,” *Applied Thermal Engineering*, vol. 26 (7), pp. 709-719, 2006.
[20] J. Nocedal and S.J. Wright, “Linear Programming: The Simplex Method”, Chapter 13 in *Numerical Optimization* (second edition), Springer Series in Operations Research, Springer Verlag, 2006.